JCTC Journal of Chemical Theory and Computation

A Theoretical Study of Brominated Porphycenes: Electronic Spectra and Intersystem Spin−Orbit Coupling

Angelo Domenico Quartarolo, Sandro Giuseppe Chiodo, and Nino Russo*

Dipartimento di Chimica and Centro di Calcolo ad Alte Prestazioni per Elaborazioni Parallele e Distribuite—Centro d'Eccellenza MIUR, Università della Calabria, I-87030 Arcavacata di Rende, Italy

Received June 1, 2010

Abstract: In this paper, a time-dependent density functional theoretical study (TDDFT) has been carried out for brominated 2,7,12,17-tetra-*n*-propylporphycenes. Their potential therapeutic use in photodynamic therapy (PDT), a noninvasive medical treatment of cancer diseases, is due to the strong absorbance in the red part of the visible spectrum and the presence of heavy atoms (bromine). The prediction of electronic spectra for photosensitizer molecules can be a valuable tool in the design of drugs for application in PDT. Singlet and triplet vertical excitation energies have been calculated by means of the nonempirical hybrid functional PBE0 in conjunction with a split valence basis set (SVP), on previously optimized, at the density functional level of theory, ground state geometries. In particular, the quantum-chemical simulation of their absorption electronic spectra, both *in vacuo* and in solvent environments (dichloromethane and bromobenzene), has evidenced the red shift maxima wavelengths for the Q bands (or lower energy bands) with an increasing number of bromine atoms, in agreement with experimental results. The mean absolute deviation for the Q-electronic bands is about 0.3 eV. Calculated vertical triplet energies are between 1.04 (for tetra-brominated derivative) and 1.20 eV (for dibrominated derivative). The influence of bromine atoms on intersystem spin crossing has been investigated by applying a computational code which calculates spin−orbit matrix elements between singlet and triplet excited state wave functions weighted by the TDDFT transition coefficients.

1. Introduction

Porphycene is a nonporphyrin tetrapyrrolic macrocycle and the first constitutional isomer of porphyrin reported in the literature, having an 18 π-electron planar conjugated system.[1] This compound was first synthesized by Vogel and co-workers in 1986 by means of the McMurry coupling of bipyrrole dialdehydes.[2,3] Although the synthesis of porphycene is generally low-yielding, its unique optical features and in particular the strong absorption in the far-red part of the visible region have attracted chemical researchers to the synthesis of new derivatives for application in the medical area of photodynamic therapy (PDT).[4] PDT is a noninvasive technique for the treatment of different kinds of tumors (e.g., early lung, breast, and prostate cancers), age-related macular degeneration (AMD), and skin diseases.[5−8] The combination of a laser light source, a photosensitizer drug dose, previously injected in the human body, and the presence of molecular oxygen $^3O_2$ ($^3\Sigma_g^-$), naturally present in human tissues, can induce apoptosis and/or necrosis of tumoral cells as a result of *in locu* generated cytotoxic oxygen species.[9,10] The mechanism of generation of singlet oxygen $^1O_2$ ($a^1\Delta_g$) as the key cytotoxic agent, which is usually referred to as the type II PDT mechanism, involves a cascade of photochemical steps.[11−13] First, the photosensitizer in its ground state S_0 is excited to the first excited state S_1 state by irradiation with a wavelength, preferably in the so-called therapeutic window between 600−900 nm, that should overlap the maximum absorption wavelength of the sensitizer.[14] Red-shifted absorption wavelengths are preferred since they better penetrate

* To whom correspondence should be addressed. E-mail: nrusso@unical.it.

10.1021/ct100287g
Published on Web 09/07/2010

Scheme 1. Molecular Structures and Atom Numbering

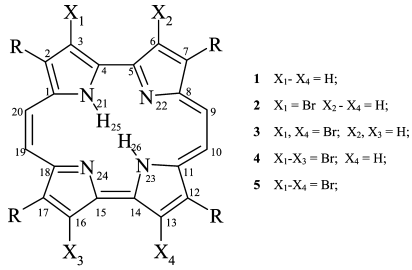

1 X_1- X_4 = H;
2 X_1 = Br X_2 - X_4 = H;
3 X_1, X_4 = Br; X_2, X_3 = H;
4 X_1-X_3 = Br; X_4 = H;
5 X_1-X_4 = Br;

1 - 5

human tissues, allowing the treatment of deeper tumors. In the type II mechanism, the S_1 state of the sensitizer decays to the first triplet excited state (T_1), through a radiationless transition or intersystem spin crossing process (isc), and the energy gain is then transferred to molecular oxygen, forming the highly reactive species $^1O_2$. The latter step requires an activation energy of about 0.98 eV, which corresponds to the $^3\Sigma_g^- \rightarrow {}^1\Delta_g$ electronic transition for molecular oxygen.[15] The efficiency of a photosensitizer as a PDT drug mainly depends on its electronic absorption spectrum features, such as maximum wavelength positions and intensities, and on the ability to generate $^1O_2$. The latter factor is measured by the singlet oxygen quantum yield (Φ_Δ) of the sensitizer and is related to the electron transfer process. Other structural factors, like the photosensitizer amphiphilic character or the possibility to form aggregates in aqueous solution which decrease the photodynamic action, play an important role in the PDT drug design. The attempt to increase the value of Φ_Δ can be searched for by introducing heavy atoms, such as halogens (Br, I) or transition metal atoms in the molecular structure. The presence of a heavy atom (high atomic number) causes the mixing of pure electronic states of different spin multiplicities (the so-called heavy atom or spin−orbit coupling effect), increasing the rate of isc between S_1 and T_1 states ($S_1 \rightarrow T_1$ radiationless transition).[16−18] When the triplet lifetime is sufficiently long-lived (typically on the order of few microseconds) in order to avoid deactivation by solvent molecular collisions, the energy transfer from the T_1 photosensitizer state to $^3O_2$ is favored, and consequently Φ_Δ increases. Currently, photosensitizers approved for clinical use belong to the porphyrin-like class of molecules.[19,20] Photophrin, a mixture of hematoporphyrin monomers, dimers, and oligomers, was the first accepted PDT drug for the treatment of early stage lung cancer.[21] Other synthetic photosensitizers like *m*-tetrahydroxyphenylchlorin (mTHPC, Foscan)[22] and lutetium texaphyrin (Lutrin)[23,24] have been accepted for clinical use. However, also, the synthesis of new nonporphyrin potential PDT drug (e.g., phenotiazinium, tetra-aryl-azadipyrromethenes, or hypericin derivatives) represents an important growing research field.[25−29] In this paper, we will present a theoretical study of the structures and photophysical properties of brominated 2,7,12,17-tetra-*n*-propylporphycenes (Scheme 1, structures **2**−**5**) along with the corresponding unsubstituted molecule (Scheme 1, structure **1**). The chemical synthesis of the brominated compounds, described in previous papers, provides the formation of mono-, di-, tri-, and tetra-brominated porphycenes according to the amount of bromine added to compound **1**.[30−33] The experimental study by Shimakoshi et al. of the photophysical properties (absorption, fluorescence, and phosphorescence spectra as well as their quantum yields) revealed the dependence of these properties on the number of bromine atoms.[33] In particular, the rate of isc (k_{isc}), which measures the efficiency of the $S_1 \rightarrow T_1$ radiationless transition, is at a maximum for the tetra-brominated porphycene and increases with the number of bromine atoms, confirming the role of the heavy atom effect on these compounds. The experimental values of Φ_Δ for the brominated derivatives range from 0.49 (**5**) to 0.95 (**2**) and are higher than the corresponding value of the unsubstituted structure **1** ($\Phi_\Delta = 0.36$).[33,34] Theoretical calculations can usually predict and rationalize electronic spectra and wavelength shift depending upon the nature of the substituent. This fact can be useful for the molecular design of red-shifted PDT photosensitizers, taking advantage from the prediction of absorption electronic spectra by means of time-dependent density functional theory (TDDFT).[35] In the past decade, this theoretical methodology for electronic excited states has became an efficient and routine tool for predicting electronic spectra even for large molecules.[36−38] Moreover, in the computational approach for the study of electronic excited states, it is also possible to have theoretical insights about the isc mechanism. In fact it is well-known from the application of perturbation theory to radiationless transitions that the $S_1 \rightarrow T_1$ transition depends quadratically on the corresponding matrix element of the spin−orbit quantum operator H_{so}. For this purpose, a computational code has been developed in our lab, for the calculation of the H_{so} matrix elements between two reference wave functions with different spin multiplicities. In our case, we are interested particularly in the S_1 and T_1 electronic excited states. In a first approximation, the knowledge of these elements can be correlated to the constant rate k_{isc}, giving some preliminary hints about the photosensitizer's ability to populate the triplet state and act as a PDT drug.

2. Theoretical Approach for Spin−Orbit Contributions

One particular application of our recently developed[39,40] method is an occasionally useful way to evaluate the SO matrix elements between the S_i and T_j states. In the following, we shortly describe the strategy, actually in use by us, for calculating these contributions. A good hint is furnished by this expression:

$$\langle S_i|H_{SO}|T_j\rangle = \sum_{l}^{N_{Si}} \sum_{m}^{N_{Tj}} C_{il}^{S} C_{jm}^{T} \langle \Psi_{il}^{S}|H_{SO}|\Psi_{jm}^{T}\rangle \qquad (1)$$

where Ψ^S and Ψ^T are the singlet and triplet state wave functions, respectively, arising from one-electron vertical excitations performed over the ground state (S_0) electronic configuration, $C_{il}{}^S$ and $C_{jm}{}^T$ are the coefficients of the *l*th one-electron singlet transition and *m*th one-electron triplet transition belonging to the S_i and T_j states, respectively. N_{Si} and N_{Tj} are the number of transitions defining the *i*th and *j*th singlet and triplet states, respectively. H_{SO} is the full Breit−Pauli operator.[41] More advanced discussion about the

approach used to compute the SO matrix elements between the Ψ^S and Ψ^T wave functions can be found elsewhere.[38,39] However, the used approximation that is entered in the expression (eq 1) is based on the TD-DFT assignment ansatz,[34] which has been shown to be exact to linear order for some matrix elements between ground and excited states.[42,43] But to achieve accuracy up to linear order, the second order response of the density has to be taken into account.[44] However, this ansatz is widely used for matrix elements between excited states with satisfactory results.[45]

Notice that each set of the coefficients C_{il}^S and C_{jm}^T, of which their squared values symbolically are reported in Tables 4 and 6 as c^2, comes from TD-DFT calculations.

Not as well appreciated as it ought to be is the fact that, despite the size of the molecules investigated, this procedure uses the full and exact Breit−Pauli operator instead of an approximate one. But the expression (eq 1) could not necessarily be the most efficient or fastest executing one, due to the large number of terms that could be enclosed. Thus, one can, in principle, easily find a good approximation by simply truncating the expression (eq 1) to a few terms, those belonging to larger values of the weighted coefficients, making it easier to evaluate. In this work, we have not used the full set of coefficients and the corresponding transitions defining the singlet, Ψ^S, and triplet, Ψ^T, wave functions but the main configurations belonging to the higher values of their squared coefficient, c^2, as listed in Tables 4 and 6.

It is worth emphasizing that the strategy for finding SO matrix elements between S_i and T_j states assumes that singlet, Ψ^S, and triplet, Ψ^T, wave functions are built from molecular orbitals (MO) of the ground state S_0, without invoking all the machinery beyond the separate optimization of these wave functions. Their electronic configurations are defined according to the TD-DFT results by simply promoting one electron from an occupied orbital to an unoccupied one.

Open shell singlets are obtained as a combination of $\alpha\beta$ and $\beta\alpha$ wave functions:

$$2^{-1/2}[\alpha\beta - \beta\alpha] \tag{2}$$

and, concerning the triplets, as $\alpha\alpha$ and $\beta\beta$ wave functions and, as before, by a combination of $\alpha\beta$ and $\beta\alpha$ ones:

$$\alpha\alpha, 2^{-1/2}[\alpha\beta + \beta\alpha], \beta\beta \tag{3}$$

Supposing there is *a priori* knowledge about previous works concerning our SO basic method,[39] often it is a workable procedure to biorthogonalize the MOs of different states coming from separate optimizations. But here, occasionally, we have switched off the biorthogonalization, since, as hinted, the MOs of the singlet, Ψ^S, and triplet, Ψ^T, wave functions, being unaltered from the S_0 ground state wave function, are already biorthogonals. Nevertheless, in doing so, it is needed, very often, to reorder the MOs in such a way that the discoincident orbitals, the orbitals involved in the coupling mechanism, must be shifted to external ones, as HOMO orbitals (without changing the MOs' occupation of the singlet, Ψ^S, and triplet, Ψ^T, wave functions), as required in the implementation of MOLSOC code.[39,40] But, due to this operation, it is absolutely necessary to assign the right sign for the wave function, because of the antisymmetrization principle.

3. Computational Details

Structure optimizations and excitation energies were calculated by means of the TURBOMOLE quantum chemistry program (version V5.10).[46] Gas-phase ground state geometry optimizations were carried out at the density functional level of theory. For that purpose, the nonempirical PBE0 hybrid functional was employed, which includes a fixed amount (1/4) of the exact Hartree−Fock exchange energy to the gradient-corrected PBE exchange-correlation functional.[47,48] For structure optimization calculations, the Stuttgart effective-core quasi-relativistic pseudopotential (SDD, 28 core electrons) and the corresponding optimized basis set for valence electrons (ecp-28-mwb: (6s6p1d)/[3s3p1d]) were assigned to Br atoms.[49] The standard split valence basis set, with one set of polarization functions added, was used for C, N (SVP: (7s4p1d)/[3s2p1d]), and H (SVP: (4s1p)/[2s1p]).[50] Pseudopotential and basis sets were taken from the TURBOMOLE basis set library. A vibrational frequency analysis performed at the same level of theory confirmed the stationary points found as potential energy surface minima.[51] Single point energy calculations, for the *cis* and *trans* optimized tautomers of Scheme 1, were done with the recently developed double-hybrid functional B2PLYP in conjunction with the resolution of identity approximation and the polarized valence triple-ζ basis set (TZVP).[52,53] The B2-PLYP functional gives high accuracy for noncovalent interactions with a mean absolute deviation between 0.2 and 0.3 kcal/mol and can better assess the most stable tautomer.[54] Linear response properties (singlet and triplet excitation energies) were calculated on the ground state equilibrium structures, by means of time-dependent density functional theory (TD-DFT)[55] and the same basis set (SVP) for all atoms (Br, N, C, H). The simulation of the UV−vis electronic spectra band shape was made by convolution of the first 20 singlet excitation energy roots with Gaussian functions having a constant full-width at half-maximum of 0.2 eV, using the SWizard program.[56] Bulk solvation effects on ground state geometries and excitation energies were included by means of the conductor-like polarizable model (COSMO).[57] For this reason, the dielectric constant of dichloromethane ($\varepsilon = 8.93$) with a solvent radius of 2.27 Å was manually set, while optimized atomic radii and other default parameters for the cavity construction were taken from the COSMO module. For the calculation of triplet energies, bromobenzene ($\varepsilon = 5.4$) has also been considered as a solvent, doing single point energy calculations on the gas phase optimized structures. Some calculations of excitation energies have also been performed with two recently developed hybrid meta-GGA functionals (BMK and M06−2X)[58,59] and the GAUSSIAN 03 program.[60]

SO matrix elements have been evaluated using the MolSOC[39,40] code interfaced with the TURBOMOLE program package.[46] The *mos* file of TURBOMOLE containing the coefficients of the MOs, the basis set file, and the input file, containing a route section (specifying the keywords), a charge and multiplicity section, and a geometry section are necessary for carrying out SO calculation with MolSOC. As

Scheme 2. Tautomeric Equilibria between *trans* (**B** and **D**) and *cis* (**A** and **C**) Configurations in Porphycene

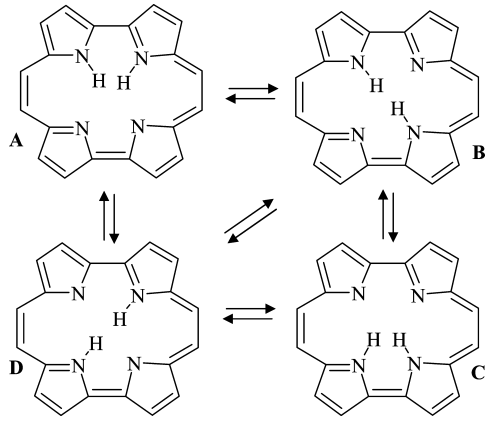

mentioned above, the MOs of the Ψ^S and Ψ^T wave functions (expression 1) are those of the ground state, S_0. These have been optimized at the PBE0/SVP level.

4. Results and Discussion

The following discussion is divided into four parts containing (a) the molecular structure and energetic aspects of brominated porphycenes (section 4.1), (b) one-electron absorption electronic spectra, (c) triplet energies (section 4.2), and (d) the efficiency of the $S_n \rightarrow T_n$ intersystem spin crossing mechanism as derived from spin−orbit matrix elements analysis (section 4.3).

4.1. Ground State Structure Properties. Porphycenes display a reduced inner cavity in comparison to porphyrins, and for that reason the inner pyrrolic hydrogens can undergo faster ground-state tautomerization between the adjacent (ethylenic bridged) pyrrole rings (see Scheme 2).[61] This process is also favored by the formation of strong intramolecular hydrogen bonds (as for example between $N_{21}-H_{25}\cdots N_{24}$ atoms of Scheme 1). The proposed mechanism of tautomerization in porphyrins, as deduced by nuclear magnetic resonance (NMR) studies, implies the interconversion between the *trans* and *cis* conformations of the four inner hydrogens, through a sequence of one-step processes.[62] The thermal activated hydrogen transfer between opposite pyrrole rings, leading to *trans* to *cis* conversion, can be followed by the formation of the other *trans* conformation or a reversal process to the initial *trans* structure. An equivalent representation of this process, describing the interconversion between tautomeric forms in porphycene, is reported in Scheme 2. The extent of the interconversion mechanism mainly depends on the energetic barriers among the different tautomeric forms. In order to assess the most stable tautomer to adopt for all subsequent response property calculations, an energetic analysis was performed for the *cis* and *trans* tautomeric forms of compounds **1**−**5**. All four tautomers (both *trans* and *cis* species) are found to be local energy minima. The absolute (atomic units) and relative calculated energies (kcal/mol), with respect to the most stable tautomer found within the mono-, di-, tri-, and tetrabrominated porphycene series (**2**−**5**) as well as for the tetra-propylporphycene (**1**), are reported in Table 1. From gas-phase PBE0 calculations, the most stable tautomer form was found to be, in all cases, the *trans* configuration. The energetic trend was also supported by single point energy calculations with the B2PLYP/TZVP approach. Notwithstanding the stability of *trans* molecular structures, the difference between *trans* and *cis* tautomers is lower than 4 kcal/mol. So the energetic barrier of these compounds can be easily overcome, in particular in liquid media, through the energy transfer mechanism due to molecular collisions. A potential energy profile *in vacuo*, relative to the different tautomers of monobrominated porphycene **2**, has been depicted in Figure 2. The connection between *trans* and *cis* ground state equilibrium structures goes through the formation of transition states, which have been found for the *trans* **D** and **B** tautomers to the *cis* **A** and **C** ($\mathbf{TS_{D-A}}$, $\mathbf{TS_{D-C}}$, $\mathbf{TS_{B-A}}$, and $\mathbf{TS_{B-C}}$ molecular structures in Figure 1). The transition state structures correspond to a hydrogen-transfer process between the two pyrrolic rings connected by the ethylenic bridge. The interconversion barrier energies, between the *trans* **D** structure to the *cis* **A** and **C** forms, are respectively 4.0 and 3.4 kcal/mol with the corresponding N−H stretching imaginary frequencies of 1030*i* and 1060*i* cm^{-1}. For the transition state $\mathbf{TS_{D-A}}$ (likewise for $\mathbf{TS_{D-C}}$), the equilibrium bond lengths found between the exchanged hydrogen and pyrrolic nitrogens are slightly asymmetrical, being respectively 1.235 and 1.331 Å ($N_{21}-H_{25}$ and $N_{24}-H_{25}$ distances of Scheme 1). For *trans* **B** structure interconversion to *cis* **A** and **C**, the energy barriers are respectively 2.66 and 2.99 kcal/mol with imaginary frequencies of 1072*i* and 1112*i* cm^{-1}. The low energetic barriers found are compatible with the simultaneous presence in solution of the *cis* and *trans* forms, with the latter being the dominant tautomeric form. From fluorescence polarization experiments on bare porphycene, the *trans* configuration resulted to be dominant in both S_0 and S_1 states.[61] This technique also allows the determination of tautomerization rates through the analysis of emission anisotropy values. For porphycene, in the S_1 state, a double-hydrogen transfer or *trans*−*trans* conversion has been observed as the interconversion step and is faster than the *cis*−*trans* mechanism.[63] Double-hydrogen transfer (or tunneling) is also valid for the ground state, as demonstrated in a previous study at cryogenic temperatures for 9-acetoxy-2,7,12,17-tetra-*n*-propylporphycene.[64]

The approach that can be used to explain the tunneling effect depends mainly on three factors: (a) the energy difference between the ground state equilibrium structures (*trans*), which can interconvert through the double-hydrogen transfer reaction, (b) the energetic transition state barrier height, and (c) the distance of pyrrolic hydrogen between the two *trans* structures (or interminimal distance). Low values of each of these factors can promote the tunneling. For the above-mentioned 9-acetoxy-2,7,12,17-tetra-*n*-propylporphycene molecule, lying in the ground state, factors a and b have been estimated to be respectively less than 180 cm^{-1} (0.5 kcal/mol) and 1820 cm^{-1} (5.2 kcal/mol). So despite the asymmetric molecular structure for the two *trans* tautomers, due to the acetoxy substituent, these low values allow hydrogen atoms to tunnel directly through the double-minimum potential energy in competition with the *trans* to *cis* tautomerization step. In the case of porphycene derivative

Table 1. Absolute (hartree) and Relative Electronic Energies (kcal/mol) for *trans* and *cis* Tautomeric Forms of Compounds **1**−**5**, Calculated at the PBE0/(SVP-SDD) and B2PLYP/TZVP Levels of Theory[a]

molecule		tautomer **1**[b]	tautomer **2**[b]	tautomer **3**[c]	tautomer **4**[c]
1	PBE0/SVP	−1458.595004	−1458.595017	−1458.592111	−1458.592111
		(0.01)	**(0.00)**	(1.82)	(1.82)
	B2PLYP/TZVP[d]	−1460.247910	−1460.247894	−1460.244038	−1460.244033
		(0.0)	(0.01)	(2.42)	
2	PBE0/SVP	−1472.128805	−1472.131124	−1472.126145	−1472.127534
		(1.526)	**(0.00)**	(3.12)	(2.25)
	B2PLYP/TZVP	−4033.401372	−4033.403637	−4033.397691	−4033.398977
		(1.42)	(0.00)	(3.73)	(2.92)
3	PBE0/SVP	−1485.666347	−1485.661807	−1485.660664	−1485.660664
		(0.00)	(2.85)	(3.57)	(3.57)
	B2PLYP/TZVP	−6606.556697	−6606.552295	−6606.549926	−6606.549927
		(0.00)	(2.76)	(4.25)	(4.25)
4	PBE0/SVP	−1499.183369	−1499.185844	−1499.179813	−1499.181718
		(1.55)	**(0.00)**	(3.78)	(2.59)
	B2PLYP/TZVP	−9179.696892	−9179.699194	−9179.692054	−9179.694702
		(1.44)	(0.00)	(4.48)	(2.82)
5	PBE0/SVP	−1512.703398	−1512.703249	−1512,698968	−1512.698862
		(0.00)	(0.01)	(2.78)	(2.75)
	B2PLYP/TZVP	−11752,837861	−11752.837658	−11752.832882	−11752.832710
		(0.00)	(0.13)	(3.12)	(3.23)

[a] Energy minima are denoted in parentheses in bold character. [b] *trans* configuration. [c] *cis* configuration. [d] Single point energy calculations at PBE0/SVP (H, C, N)-SDD (Br) optimized geometries.

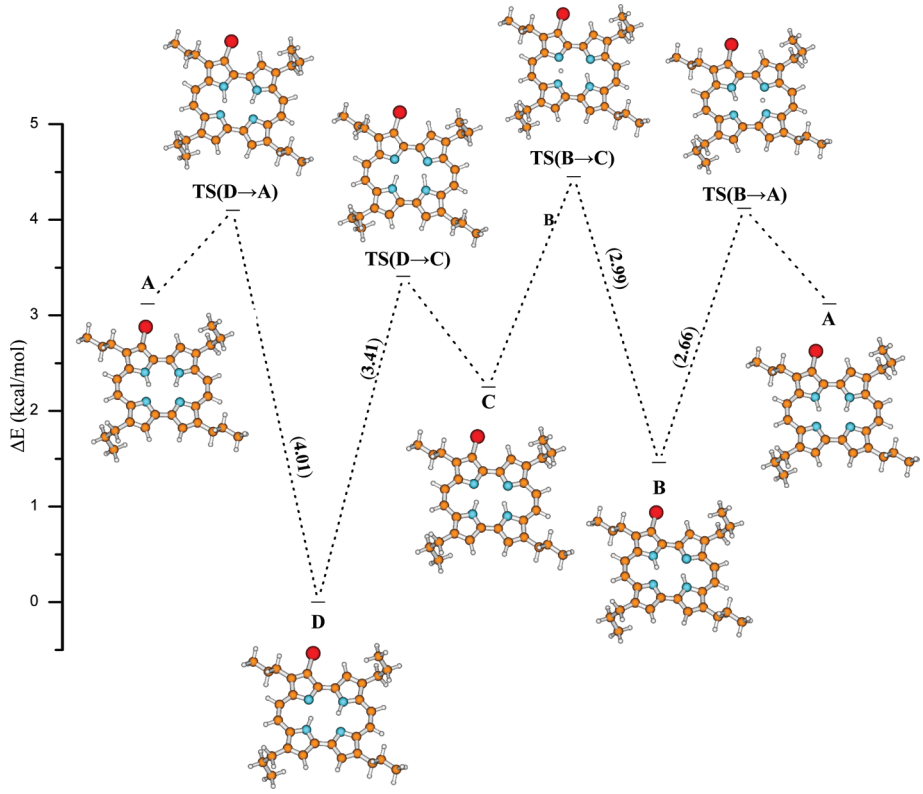

Figure 1. Energy profile and molecular structures (minima and transition states) for the interconversion between the tautomeric forms **A**−**D** of Scheme 1 for molecule **2**. In parentheses are reported the energy barriers (kcal/mol) between *trans* and *cis* tautomers. The most stable tautomer (structure **D**) is taken as the zero-energy reference.

2, the evaluation of the energetic barrier for the transition state corresponding to the double-hydrogen transfer can give insights into the possibility of tunneling for this class of brominated porphycenes. Some attempts to find for compound **2** this hypothetical transition state with the two inner hydrogens equidistant from the pyrrolic nitrogens have not been successful. This fact is probably due to the asymmetric chemical environment for the inner hydrogens, which cause the starting geometry to revert to the $\mathbf{TS_{D-C}}$ or $\mathbf{TS_{B-C}}$ transition state final geometries. A different strategy adopted for finding an approximate energy value for this hypothetical state was to perform a potential energy surface scan versus the two N−H distances. These distances were increased simultaneously by 0.1 Å, starting from the *trans* equilibrium ground state geometry of tautomer **D**. During the scan energy calculation, pyrrolic nitrogen and hydrogen Cartesian coor-

Table 2. Bond Lengths (Å) and Valence and Dihedral Angles (deg) for Brominated Porphycenes[a]

	2		3		4		5	
	calcd	$\Delta^{exp-calcd}$	calcd	$\Delta^{exp-calcd}$	calcd	$\Delta^{exp-calcd}$	calcd	$\Delta^{exp-calcd}$
				Bond Length				
C_3-X_1	1.837	(0.013)			1.827	(0.033)	1.826	(0.05)
C_6-X_2			1.836	(0.039)	1.832	(−0.029)	1.832	(0.042)
$C_{16}-X_3$			1.836	(0.039)	1.836	(−0.033)	1.832	(0.035)
$C_{13}-X_4$							1.826	(0.054)
C_4-C_5	1.415	(0.009)	1.413	(−0.005)	1..424	(−0.005)	1.420	(0.006)
$C_{19}-C_{20}$	1.391	(−0.006)	1.391	(0.002)	1.386	(−0.032)	1.387	(−0.008)
$C_{20}-C_1$	1.411	(−0.001)	1.403	(0.001)	1.406	(0.01)	1.403	(0.003)
C_1-C_2	1.457	(0.015)	1.443	(−0.006)	1.432	(−0.022)	1.432	(0.007)
C_2-C_3	1.368	(0.013)	1.378	(−0.014)	1.381	(−0.022)	1.380	(−0.009)
N_1-C_1	1.355	(−0.014)	1.360	(0.006)	1.361	(0.013)	1.359	(0.014)
N_1-C_4	1.346	(0.023)	1.357	(0.012)	1.363	(−0.009)	1.363	(−0.007)
MAD[b]	0.01		0.01		0.02		0.02	
rms[b]	0.01		0.02		0.02(5)		0.03	
				Bend Angle				
$C_1-N_1-C_4$	107.91	(−0.44)	110.42	(−0.35)	111.33	(−4.04)	111.31	(−3.3)
$C_{19}-C_{20}-C_1$	132.21	(−0.79)	131.15	(−0.27)	131.77	(0.12)	131.01	(1.12)
				Dihedral Angles				
$C_3-C_4-C_5-C_6$	−0.137	(0.5)	−0.080	(0.7)	−0.707	(3.5)	−20.857	(6.0)
$C_{13}-C_{14}-C_{15}-C_{16}$	0.078	(0.6)	0.075	(0.7)	21.863	(17.7)	−20.879	(2.0)

[a] In parentheses are reported the deviations ($\Delta^{exp-calcd}$) from X-ray experimental data. [b] Absolute mean deviation (MAD) and root-mean-square deviation (rms).

dinates were kept fixed while the remaining parameters were fully optimized. The energy versus N−H coordinate plot, reported in the Supporting Information (Figure S1, S14), gave an approximate high energy barrier of about 16 kcal/mol, which is greater than the energy required for the *trans*−*trans* interconversion mechanism by a two-step transfer mechanism. Similar results have been obtained for compound **5** (Figures S2, Supporting Information), which has a more symmetrical chemical environment and a lower *trans*−*trans* energy gap. In this case, the energy barrier height is even higher (about 30 kcal/mol).

The energetic stability of the *trans* conformations in comparison to that of the *cis* can be mainly ascribed to different geometrical parameters inside the inner cavity, which in turn can mutually influence the energy contribution of intramolecular hydrogen bonds. For instance, in *trans* conformations, the inner hydrogen distance is slightly greater than in the *cis* by about 0.02 Å; similarly the increase of the opposite nitrogen distance implies an overall minor sterical hindrance inside the cavity. It can be noted from Table 1 that in compounds **1** and **5**, for which inner hydrogen atoms show a similar chemical environment by symmetry, the *trans* tautomers have about the same electronic energy, and the same holds for the *cis* forms. In the same way, the presence of bromine substituents and in particular the proximity to pyrrolic hydrogens can account for the small energy difference between each *trans* or *cis* tautomeric pair by the electron-withdrawing effect, which induces a different electronic charge distribution on the molecular system. A list of some geometrical parameters (bond lengths, valence and torsional angles) for the most energetically stable tautomer of each porphycene derivative (**2**−**5**) is presented in Table 2. For bond lengths, the agreement with the experimental data has been evaluated by means of the absolute mean deviation (MAD) and the root mean squared deviation (rms) values. For both statistical descriptors, the bond length deviation for all compounds ranges between 0.01 and 0.03 Å, showing a good agreement with experimental data. Bend and torsional angles are generally described with an accuracy within 6°, except for compound **4**, where the steric repulsion between vicinal bromine atoms is described theoretically by a torsion displacement between adjacent pyrrolic rings by about 22° (angle $C_{13}-C_{14}-C_{15}-C_{16}$). On the other hand, crystallographic measurements gave an angle of *ca*. 4°, due to the formation of intermolecular π-stacking interactions which are responsible for the coplanarity between the rings.[33] In the present discussion, we have implicitly omitted the existence of the two other possible *cis* tautomers having the inner pyrrolic hydrogens connected on the same side of the ethylenic bridges (bonds $C_{19}-C_{20}$ and C_9-C_{10} in Scheme 1). In fact, from preliminary optimization calculations on compound **2**, their relative energies lie well above the *trans* stable tautomeric forms by about 90 kcal/mol. For that reason, their influence on molecular properties, with a good approximation, can be neglected in comparison with the more stable *trans* and *cis* structures reported in Scheme 2.

4.2. Bromine Effect on Electronic Absorption Spectra. The electronic spectra of porphyn and porphyrin-like systems (e.g., chlorine and bacteriochlorin) can be interpreted by means of the so-called four-orbital model proposed in the early 1960s by Gouterman and co-workers and based on semiempirical theoretical calculations.[65,66] The main features of the electronic bands in the UV−visible region of the spectrum are described as excitation electronic transitions between the occupied (HOMO and next-HOMO, hereafter called H and H−1) and the unoccupied (LUMO and next-LUMO, or L and L+1) molecular frontier orbitals. For the free-base porphyn, the electronic spectrum consists of a series of absorption bands between 500 and 600 nm (Q bands) of weak intensity (molar absorptivity $\varepsilon \sim 10\,000\ M^{-1}\ cm^{-1}$) and a more intense band near the UV region at about 400

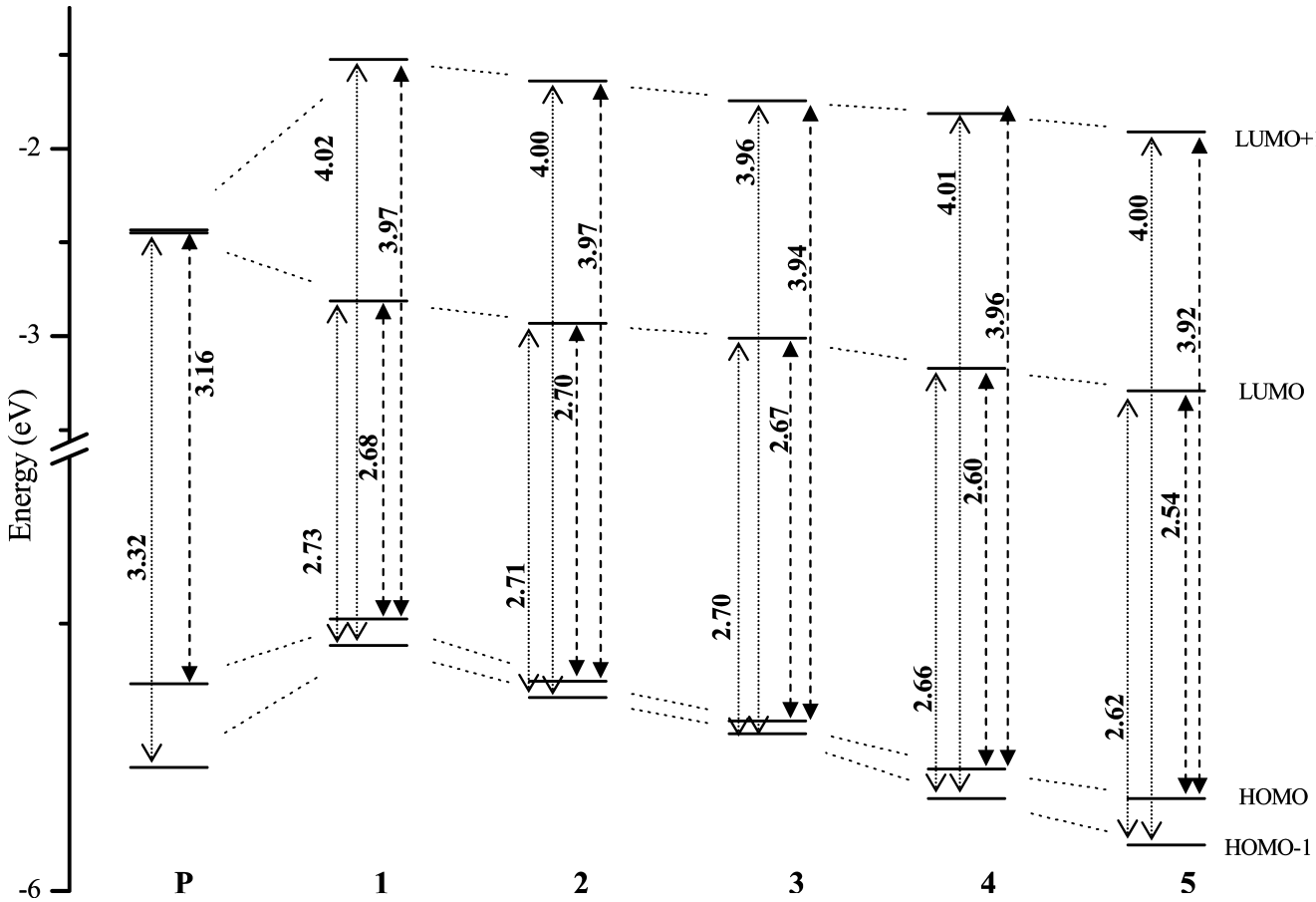

Figure 2. Frontier molecular orbital energy diagram for porphyn (**P**) and molecules **1**−**5**. Gap energies (eV) between H−1 to L/L+1 (dot arrow) and H to L/L+1 (dash arrow) are also shown.

nm (called B or Soret bands, $\varepsilon \sim 200\,000$ M^{-1} cm^{-1}).[6,65] Other electronic bands are present at higher energies (between 3.65 and 5.50 eV) and are classified according to Platt's nomenclature as N, L, and M bands.[67] The proposed explanation for the weak intensity of the electronic Q bands (denoted as Q_x and Q_y) in porphyrin is related to the equal weight of the two transition configurations which compose each Q band and to the near-degeneracy of the orbital energies of the final states (next-LUMO and LUMO for **P** in Figure 2).[68] For example, the low-energy-lying Q band (Q_x, experimental energy in gas phase at 1.98 eV)[69] is described, from theoretical calculations, by similar transition coefficient weights and two distinct electronic transitions: the next-HOMO to next-LUMO and the HOMO to LUMO electronic transition. The similar but different signs of the contribution to the transition dipole moment cause its *quasi*-vanishing or weak intensity of the Q bands. A similar argument holds for the intensity of the next-excitation energy band or Q_y band (experimental gas-phase excitation energy at 2.42 eV),[69] whereas for the B bands (B_x and B_y), the two transition configurations do not cancel transition moments and strengthen the intensity of the band. In porphycene, the molecular symmetry is lower than in porphyrin (C_{2h} vs D_{2h}) and the energy splitting between the L+1 and L molecular orbitals causes the red-shift wavelength absorption and a different weight for the two Q-band electronic transitions (see for example compound **1** in Figure 2). As a consequence, the reciprocal cancellation effect on the intensity, which determines the weakness of the porphyrin Q bands, is less effective in porphycene, and the result is a stronger absorption Q band with a red-shift maximum absorption (λ_{max} = 630 nm, 1.97 eV; $\varepsilon \sim 50\,000$ M^{-1} cm^{-1} in benzene).[3] The same spectroscopic features (red-shift wavelength and strong absorption) found for porphycene are also present in its brominated derivatives **1**−**5** (see Figure 1), for which, in the following, a strict comparison between experimental and calculated data is made in order to elucidate some aspects of their electronic spectra. Before discussing the theoretical results for the most stable tautomer for each porphycene derivative, a brief comparison among the absorption electronic spectra of the different tautomers (**A**−**D** structures in Scheme 2) of compound **2** will be made. The choice of the monobromo-substituted porphycene as a test case has been made on the basis of two factors: the introduction of at least one bromine substituent with respect to porphycene derivative **1** and at the same time the low computational cost. The influence of the basis set choice (all electron or pseudopotential basis set for bromine atom) on excitation energies is shown in Table 3, where are reported the most relevant electronic bands in the visible region (Q and B bands). Among tautomers **A**−**D,** the excitation energy difference for each electronic band is generally within 0.01 eV, taking into account also the different basis sets for bromine atoms. The partial conclusion that can be deduced from this result is that the tautomerization mechanism, at least for absorption electronic spectra, does not drastically influence excitation

Table 3. Comparison between Excitation Energies ΔE in eV (Q and B bands) between the *trans* (**A**, **B**) and *cis* (**C**, **D**) Tautomers of Monobromo-Substituted Porphycene **2** (in parentheses are reported the oscillator strengths)

	A		B		C		D	
	SVP[a]	SVP/SDD[b]	SVP[a]	SVP/SDD[b]	SVP[a]	SVP/SDD[b]	SVP[a]	SVP/SDD[b]
Q_1	2.24 (0.1825)	2.24 (0.1782)	2.23 (0.1643)	2.24 (0.1686)	2.24 (0.1852)	2.24 (0.1817)	2.24 (0.1743)	2.25 (0.1753)
Q_2	2.35 (0.2614)	2.36 (0.2654)	2.35 (0.2732)	2.36 (0.2729)	2.37 (0.2413)	2.37 (0.2445)	2.33 (0.2316)	2.34 (0.2381)
B_1	3.76 (1.0411)	3.76 (1.0447)	3.75 (0.9361)	3.76 (0.9507)	3.75 (0.9209)	3.75 (0.9287)	3.74 (0.8699)	3.75 (0.8990)
B_2	3.87 (1.0380)	3.88 (10388)	3.88 (1.1311)	3.89 (1.1119)	3.86 (1.0648)	3.86 (1.0608)	3.87 (1.0311)	3.87 (1.0538)

[a] SVP all-electron basis set for all atoms. [b] SVP basis set for H, C, and N atoms and Stuttgart pseudopotential (SDD) plus optimized basis set for valence electrons for Br.

energies. So the approximation of considering the most stable tautomer for each compound as the dominant model structure present in solution, without accounting for statistically averaged tautomer populations, can offer just enough theoretical information for the electronic spectrum interpretation. The main results for the most stable tautomeric forms of compounds **1**−**5** have been reported in Table 3, including excitation energies, main transition configurations, and oscillator strengths. In particular, the results focus on Q-band trends by changing the number of bromine atoms at positions 3, 6, 13 and 16 (see Scheme 1). Since experimental absorption maxima were measured in dichloromethane, calculated bulk solvation shifts on excitation energies were also included in Table 3. It has to be noted that in the experimental spectra a third absorption peak appears in the Q-band region. From TDDFT as well as the symmetry-adapted cluster configuration interaction method (SAC−CI), there is no evidence for this electronic transition, and in previous work, it has been assigned as a Q_1 side vibrational band.[70,71] For the parent compound 2,7,15,19-tetra-*n*-propylporphycene (**1**) of brominated molecules **2**−**5**, the calculated Q bands show a slight bathochromic wavelength red-shift in comparison to the free base porphycene (**Pc**). From *in vacuo* calculations, this difference is estimated to be 10 and 6 nm, respectively, for the Q_1 and Q_2 bands. This result is the same order of magnitude as the corresponding experimental shift (5 and 4 nm), although the absorption measurements are referred to different solvents (benzene for **Pc** and dichloromethane for derivative **1**). The basic feature that emerges from the experimental absorption spectra is the red shift for the wavelength absorption of Q_1 and Q_2 bands with an increasing number of bromine atom substitutions (positions 3, 6, 13, and 16 of Scheme 1). The same findings come from theoretical calculations; in fact, both Q_1 and Q_2 bands increase in wavelength by about 37 and 25 nm, respectively, on going from compound **2** to **5**. Excitation energies, from TDDFT calculations, expressed in electronvolt units, are systematically overestimated, and the mean absolute deviation from the experimental values, for both Q_1 and Q_2 bands, is 0.3 eV, a result that is consistent with the error generally found for the hybrid TDDFT method. The oscillator strengths *f*, comprised between 0.15 and 0.3 units, are stronger than the corresponding values for porphyn calculated at the same level of theory, but less intense than the B bands which are found to be greater by about 1 order of magnitude ($f \sim 1.0$). Molecular frontier orbitals (H−1, H, L, and L+1) are mainly responsible for the electronic transitions which compose Q bands and are all $\pi\pi^*$ in character, as can be shown by plotting the relative molecular orbital isodensity surfaces (see Supporting Information, S14−S18). The main transition configuration for porphycene derivatives **1**−**5** does not follow the same transition configuration scheme shown in Table 4 for the free base porphycene **Pc**. In that case (**Pc**), the Q_1 electronic band resulted from H−1→L (78%) and H→L+1 (13%) electronic transitions, while the Q_2 band resulted from H→L (81%) and H−1→L+1 (13%). On the other hand, the Q_1 band of derivative **1** shows a non-negligible contribution from H→L (∼8%), and the Q_2 band main configuration also includes the electronic transition from H−1 to L (∼7%). At the same time for derivatives **4** and **5**, the four-orbital model is no longer completely valid since the Q_1 band of **4** and Q_2 band of **5** have minor contributions from inner orbitals (respectively H−2 and H−3). Theoretical calculations with the SAC−CI method have evidenced the failure of the four-orbital model also for the B bands of porphycene and porphyrin isomers, by proposing an alternative five-orbital model for the interpretation of their electronic spectra.[70] The Q_1 and Q_2 wavelength red shifts can be rationalized on the basis of their proper transition configuration and *in vacuo* absolute molecular orbital energies (Figure 2 and Supporting Information, S19). For instance, the Q_1 band of both **1** and **2** is mainly composed of H−1→L electronic transition by about 76% (**1**) and 82% (**2**), respectively (Table 4). The energy difference between H−1 and L slightly decreases by 0.02 eV (see Figure 2) on going from **1** to **2**, explaining the Q_1 bathochromic shift. For the derivative **3**, the energy difference between H and L molecular orbitals, with the corresponding transition being responsible by 80% for the Q_1 band, further decreases by 0.03 eV. For derivatives **4** and **5**, also considering the second electronic transition H→L, which shows a considerable weight of about 20%, the orbital energy difference decreases following the same trend as previously shown and confirming the overall Q_1 band red-shift effect from compounds **1** to **5**. The energy stabilization of L and L+1 orbitals, which decreases the energy gaps between H and L (L+1), has a greater importance for the Q-band red shift in comparison to that of H and H−1 molecular orbitals. In a similar fashion, the above interpretation scheme can be applied for explaining the Q_2 band red shift, taking into account all relevant electronic transitions contributing to that band. For example, for derivative **5**, the energy difference corresponding to the

Table 4. TDDFT Excitation Energies ΔE (eV, nm), Oscillator Strengths *f*, and Transition Main Configuration for Porphycene (**Pc**) and Compounds **1**−**5**[a]

		TDDFT						SAC−CI[b]	Expt[b]	
molecule	state	ΔE		main configuration	c^2	*f*	ΔE^{solv}	ΔE	ΔE	
Pc	1 ^{1}A	2.30,	540.1	H−1→L	0.785	0.1503	2.31	1.62	1.97	629
				H→L+1	0.135					
	2 ^{1}A	2.40,	517.2	H→L	0.812	0.2202	2.41	1.86	2.08	596
				H−1→L+1	0.126					
1	1 ^{1}A	2.25,	551.8	H−1→L	0.757	0.1649	2.25		1.96	633
				H→L+1	0.121					
				H→L	0.082					
	2 ^{1}A	2.37,	523.8	H→L	0.763	0.2721	2.36		2.06	601
				H−1→L+1	0.134					
				H−1→L	0.066					
2	1 ^{1}A	2.23,	555.9	H−1→L	0.824	0.1625	2.25		1.93	641
				H→L+1	0.110					
	2 1^1	2.35,	528.6	H→L	0.840	0.2726	2.36		2.04	607
				H−1→L+1	0.140					
3	1 ^{1}A	2.21,	562.3	H→L	0.806	0.1548	2.22		1.91	649
				H−1→L+1	0.125					
	2 ^{1}A	2.34,	530.4	H−1→L	0.836	0.2729	2.36		2.02	613
				H→L+1	0.135					
4	1 ^{1}A	2.16,	573.9	H−1→L	0.605	0.1555	2.19		1.86	665
				H→L	0.202					
				H→L+2	0.082					
				H−2→L	0.044					
	2 ^{1}A	2.29,	540.4	H→L	0.648	0.3007	2.31		1.98	625
				H−1→L	0.223					
				H−1→L+1	0.088					
5	1 ^{1}A	2.10,	589.4	H−1→L	0.556	0.1509	2.13		1.81	684
				H→L	0.250					
				H−3→L	0.089					
				H→L+1	0.071					
	2 ^{1}A	2.26,	549.6	H→L	0.613	0.3168	2.28		1.94	640
				H−1→L	0.265					
				H−1→L+1	0.076					

[b] Ref 60. [b] In dichloromethane, ref 33, except for **Pc** in benzene (ref 3). [a] Excitation energies (eV) in dichloromethane are denoted as ΔE^{solv}.

first electronic transition of Q_2 (H−1→L) is lower by 0.02 eV in comparison to that of compound **4**. At the same time for the second electronic transition (H→L, transition weight of 25%), the energy difference is greater by 0.12 eV, the overall effect being the wavelength red shift on the resulting band from **1** to **5**. This effect can also be appreciated from the simulation of the electronic spectra, obtained by overlapping with Gaussian functions for each electronic transition, showing the resulting Q_1 and Q_2 maximum absorption wavelengths (see Figure 3). The introduction of bulk solvation effects through the C-PCM method does not improve the agreement between calculated and experimental excitation energies. Moreover, Q bands appear red-shifted in wavelength only for compounds **2**−**5**, while the calculated excitation energies between **1** and **2** are identical. The performance of new hybrid meta-GGA functionals (BMK and M06−2X) on electronic excitation energies was also investigated, and the results have been are reported in Table 7. Since the mean average deviation (MAD) for both Q_1 and Q_2 bands is about 0.3 eV, these two new functionals, for the investigated systems, do not significantly improve PBE0 results.

Triplet Energies. Photosensitizer triplet energy is an important photophysical parameter in photodynamic therapy. A value above 0.98 eV is a prerequisite for energy transfer from the photosensitizer T_1 state to molecular oxygen in the type II PDT mechanism.[15] Singlet oxygen quantum yield

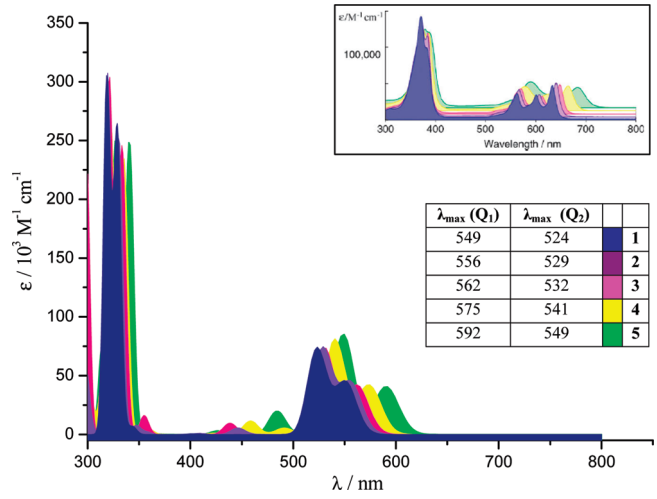

Figure 3. *In vacuo* simulated electronic spectra for molecules **1**−**5** and relative maxima absorption wavelength for Q_1 and Q_2 electronic bands. The half-height bandwidth was set to 0.2 eV. In the upper panel are reproduced for comparison the experimental spectra. Half-height bandwidths were set to 0.2 eV.

measurements reveal the efficiency of this mechanism and indirectly demonstrate that the above condition is fulfilled when singlet oxygen is experimentally detected and quantified, for example, through the peak intensity in the O_2

Table 5. Singlet ΔE ($S_0 \rightarrow S_n$, $n = 1-2$) and Triplet ΔE ($T_1 \rightarrow T_n$, $n = 1-2$) Vertical Excitation Energies and Oscillator Strengths *f* for Free Base Porphycene (**Pc**) and Derivatives **1**−**5**[a]

		BMK[b]				M06−2X[b]			
molecule	state	ΔE ($S_0 \rightarrow S_n$) (eV, nm)		*f*	ΔE($T_1 \rightarrow T_n$) (eV)	ΔE ($S_0 \rightarrow S_n$) (eV, nm)		*f*	ΔE($T_1 \rightarrow T_n$) (eV)
Pc	1	2.31	536.8	0.1803	1.10	2.26	548.8	0.1863	1.05
	2	2.42	512.5	0.2573	1.38	2.38	521.7	0.2667	1.30
1	1	2.27	545.2	0.1968	1.16	2.23	556.2	0.2107	1.12
	2	2.39	517.9	0.3102	1.40	2.35	527.6	0.3130	1.34
2	1	2.26	549.8	0.1987	1.17	2.21	561.4	0.2114	1.14
	2	2.38	521.3	0.3138	1.37	2.34	530.2	0.3222	1.31
3	1	2.23	556.2	0.1918	1.21	2.18	568.0	0.2024	1.18
	2	2.37	522.5	0.3138	1.34	2.33	531.3	0.3265	1.27
4	1	2.19	566.0	0.2044	1.11	2.15	578.0	0.2180	1.07
	2	2.33	532.4	0.3436	1.33	2.29	541.4	0.3571	1.27
5	1	2.14	580.7	0.2048	1.03	2.08	593.5	0.2193	0.98
	2	2.29	541.4	0.3583	1.32	2.25	550.7	0.3738	1.25
MAD[c]	1	0.33			0.07	0.28			0.11
	2	0.32				0.30			

[a] The values are calculated in vacuo by means of BMK and M06-2X hybrid meta-GGA functionals. [b] PBE0 optimized geometry. [c] Mean absolute deviation (MAD), in eV, for singlet ($n = 1, 2$) and triplet states ($n = 1$).

Table 6. Calculated Vertical Triplet Energies E_T (eV) *in vacuo* and in Dichloromethane ($E_T^{solv(I)}$) and Bromobenzene ($E_T^{solv(II)}$), with the Main Transition Configuration and Their Coefficients (c^2)[a]

molecule	state	E_T	$E_T^{solv\ (I)}$	$E_T^{solv(II)}$	E_T^{adiab}	main configuration[b]	c^2	exp.
1	T_1	1.16	1.19	1.19	0.73	H→L	0.930	1.27
	T_2	1.41	1.41	1.41		H−1→L	0.966	
	T_3	2.41	2.41	2.42		H−1→L+1	0.361	
						H−3→L	0.332	
						H→L+1	0.213	
	T_4	2.53	2.54	2.55		H−1→L+1	0.548	
						H−3→L	0.218	
						H→L+1	0.151	
2	T_1	1.17	1.20	1.20	0.77	H→L	0.849	1.25
						H−1→L	0.094	
	T_2	1.38	1.38	1.38		H−1→L	0.882	
						H→L	0.101	
	T_3	2.31	2.34	2.35		H−2→L	0.843	
						H→L+1	0.054	
						H−2→L+2	0.028	
	T_4	2.42	2.42	2.43		H−1→L+1	0.391	
						H−3→L	0.265	
						H→L+1	0.193	
						H−2→L	0.059	
3	T_1	1.20	1.22	1.22	0.81	H−1→L	0.930	1.24
	T_2	1.35	1.35	1.35		H→L	0.975	
	T_3	2.30	2.35	2.32		H−2→L	0.924	
	T_4	2.31	2.37	2.34		H−3→L	0.788	
						H→L+1	0.069	
						H−1→L+1	0.052	
4	T_1	1.11	1.13	1.13	0.77	H→L	0.813	1.18
						H−1→L	0.134	
	T_2	1.34	1.33	1.34		H−1→L	0.840	
						H→L	0.143	
	T_3	2.10	2.21	2.15		H−2→L	0.908	
	T_4	2.23	2.28	2.25		H−3→L	0.878	
						H→L+1	0.035	
5	T_1	1.04	1.05	1.06	0.62	H→L	0.875	1.03−1.13[c]
						H−1→L	0.075	
	T_2	1.33	1.32	1.32		H−1→L	0.902	
	T_3	2.04	2.13	2.08		H−2→L	0.930	
	T_4	2.08	2.16	2.11		H−3→L	0.904	
MAD[d]		0.07			0.46			

[a] Adiabatic triplet energies E_T^{adiab} for the first excited state and experimental phosphorescence (eV) are also given. [b] In *vacuo*. [c] Low intensity peak. [d] Mean absolute deviation (MAD), in eV, for the vertical and adiabatic T_1 state.

phosphorescence spectrum. The theoretical evaluation of the triplet energies ($S_0 \leftarrow T_1$), in the framework of the TDDFT approach, can be a valuable tool in the design of a new PDT photosensitizer. For the molecular systems just present in the literature, as is our case study, the comparison with experimental data can support or limit the applicability of a theoretical protocol. The first four TDDFT vertical triplet energies *in vacuo* have been reported in Table 6, together

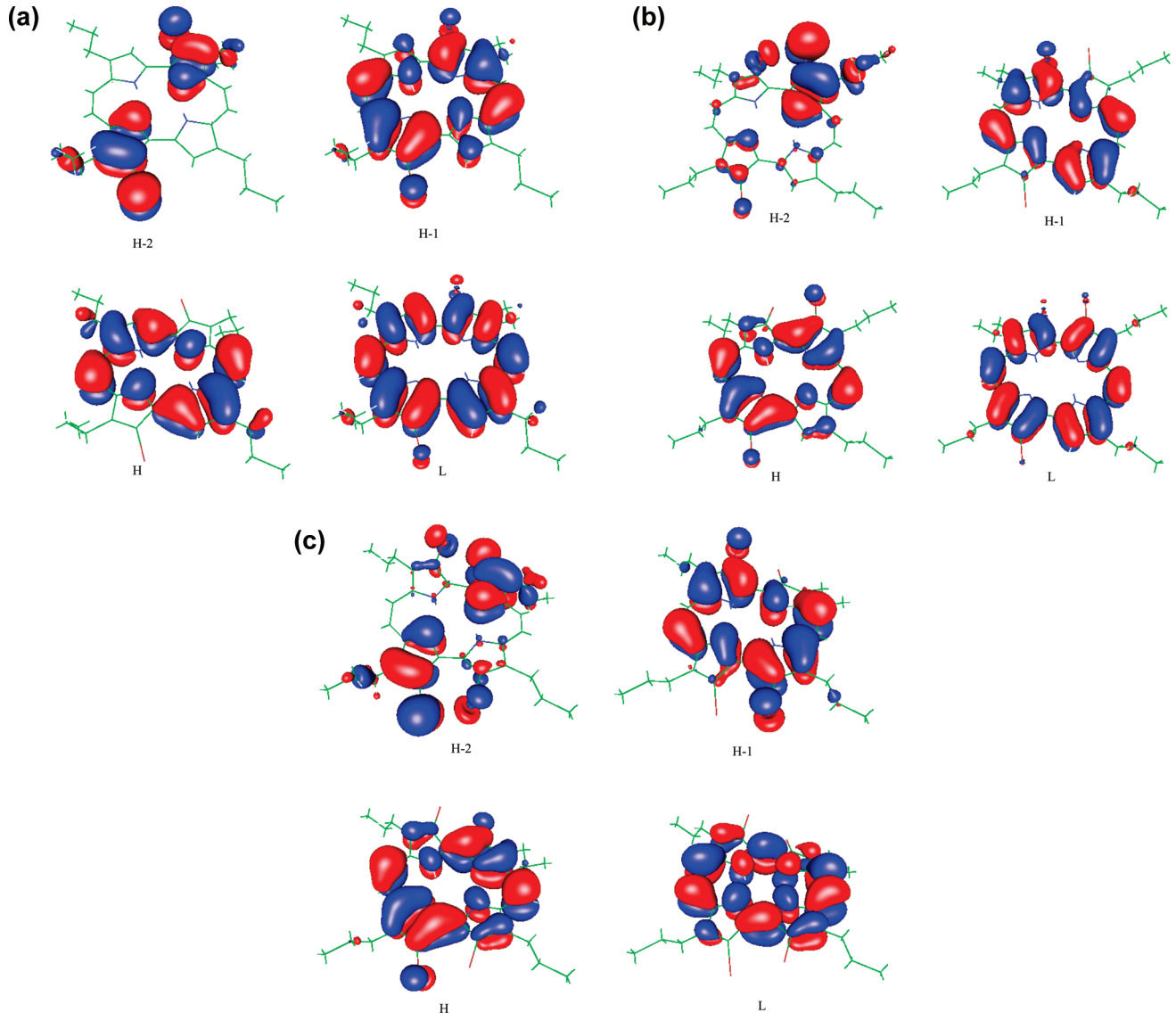

Figure 4. Graphical representation of the highest occupied and lowest unoccupied MOs for the (a) molecule **3** tautomer **1**, (b) molecule **4**, and (c) molecule **5**, obtained from the geometry of the ground states, S_0, at the PBE0 level.

with the main transition configuration and in solvent (dichloromethane and bromobenzene) values. Experimental triplet energies for derivatives **1**−**5**, as obtained from phosphorescence spectra in degassed bromobenzene, are between 1.27 and 1.03 eV.[33] All these compounds have shown appreciable singlet oxygen quantum yield Φ_Δ (between 0.36 and 0.95), a fact that confirms the strict relation between this parameter and photosensitizer triplet energies greater than 0.98 eV. The TDDFT vertical triplet energies obtained in this study cover a range between 1.20 (**3**) and 1.04 eV (**5**), with a maximum deviation of 0.1 eV from the experimental counterparts. Since phosphorescence spectra of compounds **1**−**5** refer to an emission process at the excited state relaxed geometry, it is more convenient to calculate excitation energies from the first triplet optimized geometry, in order to get a more realistic comparison with experimental data. *In vacuo* adiabatic excitation energies for the first triplet excited state of **1**−**5**, obtained in such a way, are reported as E_T^{adiab} in Table 6 and are further underestimated with respect to vertical energies with a mean absolute deviation from the experimental value of 0.46 eV. From theoretical calculations, a strict correlation between the number of bromine atoms and vertical (and adiabatic) triplet energy values has not been found in going from derivative **1** to **5**, as is the case for the experimental results where the triplet energy decreases with the number of bromine atoms. Vertical triplet energies calculated in dichloromethane and bromobenzene are almost identical and similar to *in vacuo* results. In this case, the energy deviation ranges between 0.01 and 0.03 eV. The introduction of bulk solvation effects slightly improves the agreement with experimental triplet energies (Table 6). As for the case of calculated singlet excitation energies, the mean absolute deviation for vertical triplet energies, calculated by BMK and M02−6X exchange-correlation functionals (Table 5), is comparable to that of PBE0, being respectively 0.07 and 0.1 eV.

4.3. Spin−Orbit Matrix Elements. The key concept in order to understand the trend of the SO matrix elements of the molecules investigated lies in the nature of the MOs involved in the coupling mechanism arising from the one-electron singlet and triplet transition defining the S_i and T_j states. These MOs are shown in Figure 4. Instead, the Table

Table 7. Spin−Orbit Matrix Elements (cm^{-1}) between Singlet and Triplet Excited States of Porphycene Derivatives **1**−**5** Computed Using the Geometry of the S_0 Ground State

				3			
		1	**2**	**Tau1**	**Tau2**	**4**	**5**
$\langle S_1\|H_{so}\|T_1\rangle$	*x*	0.2	0.3	2×10^{-2}	0.1	6.3	4.6
	y	0.2	0.9	0.2	1.5	10.8	9.9
	z	2×10^{-2}	0.5	1×10^{-2}	1.6	2.3	0.3
$\langle S_1\|H_{so}\|T_2\rangle$	*x*	4×10^{-2}	0.1	2×10^{-3}	3×10^{-2}	2.5	1.3
	y	5×10^{-2}	0.3	1×10^{-4}	0.9	6.8	7.8
	z	8×10^{-3}	0.2	1×10^{-4}	0.8	4.0	0.4
$\langle S_1\|H_{so}\|T_3\rangle$	*x*	6×10^{-2}	0.2	1×10^{-4}	6×10^{-2}	7.8	30.4
	y	8×10^{-2}	1.3	2×10^{-3}	3.4	33.5	0.3
	z	0.1	1.6	6×10^{-3}	2.1	11.9	4.3
$\langle S_1\|H_{so}\|T_4\rangle$	*x*	0.2	0.3	8×10^{-2}	2×10^{-4}	5.4	4.1
	y	0.1	1.6	1.2	3×10^{-3}	2.2	6.5
	z	7×10^{-2}	2.1	2.9	2×10^{-3}	6.1	1.0
$\langle S_2\|H_{so}\|T_1\rangle$	*x*	3×10^{-2}	9×10^{-2}	4×10^{-3}	3×10^{-2}	0.2	0.4
	y	5×10^{-2}	0.3	3×10^{-4}	0.8	0.8	0.9
	z	7×10^{-3}	0.2	4×10^{-4}	0.7	1.2	0.2
$\langle S_2\|H_{so}\|T_2\rangle$	*x*	0.2	0.3	2×10^{-2}	0.1	0.4	0.8
	y	0.2	0.9	0.2	1.5	4.8	2.0
	z	2×10^{-2}	0.5	5×10^{-3}	1.6	2.7	0.7
$\langle S_2\|H_{so}\|T_3\rangle$	*x*	0.1	0.2	9×10^{-4}	6×10^{-2}	26.4	17.2
	y	0.2	0.9	4×10^{-4}	1.9	21.5	7.0
	z	3×10^{-2}	0.3	4×10^{-3}	2.0	0.7	2.9
$\langle S_2\|H_{so}\|T_4\rangle$	*x*	5×10^{-2}	9×10^{-2}	0.3	5×10^{-5}	0.2	10.4
	y	0.1	0.3	2.6	3×10^{-3}	2.7	25.7
	z	3×10^{-2}	0.3	10.5	1×10^{-3}	0.8	1.4

7 listing of the SO matrix elements between S_i and T_j states, irrespective of their sign, gives several details about this matter. By analyzing the results in Table 7, we might expect an increase of the SO values as the number of substituted bromine atoms becomes larger, due to the dependence of the relativistic effects on the size of the heteroatoms. This is true for some matrix elements like the $\langle S_1|H_{so}|T_1\rangle$ when the tautomer 2 (**Tau2**) is taken into account. Nevertheless, it matters a lot whether, on the whole, this behavior is not respected, since this means that not all sites of substitution could affect the SO contributions in the same way.

What is more evident is, on the whole, the hole belonging to tautomer 1 (**Tau1**) of compound **3**, which clearly indicates that there is no benefit, as far as the SO contributions are concerned, when for this molecule the heteroatom double substitution is involved. In this case, the smallest values occur when the larger contributions to the summation above involve the same discoincident orbitals or when these are mainly located in different regions of the molecule. As an example, for $\langle S_1|H_{so}|T_2\rangle$, the coupling involves mainly the β H and the α H with coefficients of 0.90 and 0.99, respectively. Analogous considerations are held for the $\langle S_2|H_{so}|T_1\rangle$ matrix elements where the larger involved orbitals are the β H−1 and the α H−1 with coefficients of −0.91 and 0.96, respectively. The highest values belong to the $\langle S_1|H_{so}|T_3\rangle$ matrix elements of molecules **4** and **5**, respectively. Obviously, there is a more clear correlation to this fact, since, here, the MOs involved in the coupling mechanism show also a p atomic orbital contribution located in the same bromine atom. However, this is not the only reason why the SO matrix elements are enhanced. For the $\langle S_1|H_{so}|T_3\rangle$ matrix elements of compound **4**, the larger involved orbitals in the coupling mechanism are β H−2 and α H−1 with coefficients of 0.78 and −0.95, respectively, and β H−2 and α H with coefficients of 0.45 and −0.95, respectively. For the $\langle S_1|H_{so}|T_3\rangle$ matrix elements of compound **5**, the orbitals are β H−2 and α H−1 with coefficients of 0.75 and −0.96 and β H−2 and α H with coefficients of 0.50 and −0.96, respectively. Note from Figure 4b and c that in both cases the atomic orbitals of at least one of the bromines are not the same p orbitals, or p orbitals with almost the same orientation. Just these findings enlarge unconditionally the values of the SO matrix elements. Instead, concerning the $\langle S_2|H_{so}|T_3\rangle$ of tautomer 1 (**Tau1**) of molecule **3**, where larger weight is given from the coupling between the β H−2 and the α H−1 orbitals, there are still atomic orbitals centered on the heteroatom site (see Figure 4a) but with the same orientation of the p orbital involved. The best orbital orientation for SO mixing is when the two p orbitals are at 90° with respect to one another. In order to generate angular momentum, an orbital jump (as an example of the $p_z \rightarrow p_x$ type) is required.

In conclusion, for most of the matrix elements, the trend is determined by the substitution of bromine atoms. On the whole and with the exception of some case, the values of the matrix elements increase with the number of heteroatoms.

Conclusions

Ground state structures and electronic absorption spectra of 2,7,12,17-tetra-*n*-tetrapropyl porphycene and its brominated derivatives have been theoretically investigated by means of DFT and TDDFT methods. From our study, the following conclusion can be drawn:

The reduced internal cavity allows a tautomerization mechanism for the inner pyrrole hydrogens with the formation of *cis* and *trans* conformers. The most energetically stable structures are found to be the *trans* structures, though

the gas-phase energy barrier for the *trans* to *cis* interconversion is very low (within 4 kcal/mol for the monobrominated porphycene).

Optimized structure parameters, for the most stable tautomer of derivatives **1**−**5**, are in good agreement with available crystallographic data. The increasing number of bromine atoms tends to twist the torsional angle between adjacent pyrrole rings (about 20° for the tetrabrominated compound) in order to minimize sterical repulsion.

The calculated electronic spectra Q bands are red-shifted on going from the mono- to tetra-brominated porphycene derivative, as found from experimental spectra. In particular, the *in vacuo* calculated Q_1 and Q_2 maximum wavelengths are shifted respectively by 43 and 35 nm for tetrabrominated compound with respect to the unsubstituted case (compound **1**). Solvent shifts on excitation energies, as obtained from the C-PCM model, showed little difference in comparison with the calculated gas-phase ones.

The computed spin−orbit matrix elements between S_i and T_j electronic states at the ground state optimized geometry tend to increase, with the exception of some case, with the number of bromine atoms, in qualitative agreement with the experimental intersystem spin crossing rate constant trend. One exception is made by the tribrominated porphycene derivative (compound **3**), for which it is necessary to take into account also the presence of other *trans* tautomers in order to rationalize the experimental trend.

Acknowledgment. Financial support from the Università degli Studi della Calabria and MIUR (PRIN 2008) is gratefully acknowledged.

Supporting Information Available: *In vacuo* optimized structures and absolute energies (atomic units) for *trans* and *cis* tautomeric forms of compounds **1**−**5**. For the most stable tautomers, the optimized Cartesian coordinates, molecular orbital isodensity surfaces and frontier molecular orbital energies are also given. This material is available free of charge via the Internet at http://pubs.acs.org.

References

(1) Sánchez-García, D.; Sessler, J. L. *Chem. Soc. Rev.* **2008**, *37*, 215–232.

(2) Aramendía, P. F.; Redmond, R. W.; Nonell, S.; Schuster, W.; Braslavsky, S. E.; Schaffner, K.; Vogel, E. *Photochem. Photobiol.* **1986**, *44*, 555–559.

(3) Vogel, E.; Köcher, M.; Schmickler, H.; Lex, J. *Angew. Chem., Int. Ed. Engl.* **1986**, *25*, 257–259.

(4) Stockert, J. C.; Cañete, M.; Juarranz, A.; Villanueva, A.; Horobin, R. W.; Borrell, J. I.; Teixidó, J.; Nonell, S. *Curr. Med. Chem.* **2007**, *14*, 997–1026.

(5) Dougherty, T. J.; Gomer, C. J.; Henderson, B. W.; Jori, G.; Kessel, D.; Korbelik, M.; Moan, J.; Peng, Q. *J. Natl. Cancer Inst.* **1998**, *90*, 889–905.

(6) Bonnett, R. In *Chemical Aspects of Photodynamic Therapy*; Gordon & Breach Science Publishers: Amsterdam, 2000; pp 1−289.

(7) Juzeniene, A.; Peng, Q.; Moan, J. *J. Photochem. Photobiol. Sci.* **2007**, *6*, 1234–1245.

(8) Schuitmaker, J. J.; Baas, P.; van Leengoed, H. H. L. M.; van der Meulen, F. W.; Star, W. M.; van Znadwijk, N. *J. Photochem. Photobiol. B* **1996**, *34*, 3–12.

(9) Buytaert, E.; Dewaele, M.; Agostinis, P. *Biochim. Biophys. Acta* **2007**, *1776*, 86–107.

(10) Oleinick, N. L.; Morris, R. L.; Belichencko, I. *Photochem. Photobiol. Sci.* **2002**, *1*, 1–21.

(11) DeRosa, M. C.; Crutchley, R. J. *Coord. Chem. Rev.* **2002**, *233*−*234*, 351–371.

(12) Schweitzer, C.; Schmidt, R. *Chem. Rev.* **2003**, *103*, 1685–1757.

(13) Schmidt, R. *Photochem. Photobiol.* **2006**, *82*, 1161–1177.

(14) Dougherty, T. J.; MacDonald, I. J. *J. Porphyrins Phthalocyanines* **2001**, *5*, 105–129.

(15) Herzberg, G. In *Spectra of Diatomic Molecules*, 2nd ed.; Van Nostrand Reinhold: New York, 1950; pp 344−346.

(16) Darmanyan, A. P.; Foote, C. *J. Phys. Chem.* **1992**, *96*, 3723–3728.

(17) Turro, N. J. In *Modern Molecular Photochemistry*; Benjamin: Menlo Park, 1978; pp 153−198.

(18) Atkins, P. W. In *Molecular Quantum Mechanics*; Oxford University Press: New York, 1989; pp 319−343.

(19) Nyman, E. S.; Hynninen, P. H. *J. Photochem. Photobiol. B: Biol.* **2004**, *73*, 1–28.

(20) Sternberg, E. D.; Dolphin, D.; Bruckner, C. *Tetrahedron* **1998**, *54*, 4151–4202.

(21) Lipson, R. L.; Baldes, E. J. *Arch. Dermatol.* **1960**, *82*, 508–516.

(22) Ronn, A. M.; Nouri, M.; Lofgren, L. A.; Steinberg, B. M.; Westerborn, A.; Windahl, T.; Shikowitz, M. J.; Abramson, A. L. *Lasers Med. Sci.* **1993**, *11*, 267–272.

(23) Young, S. W.; Woodburn, K. W.; Wright, M.; Mody, T. D.; Fan, Q.; Sessler, J. L.; Dow, C.; Miller, R. A. *Photochem. Photobiol.* **1996**, *63*, 892–897.

(24) Hsi, R. A.; Kapatkin, A.; Strandberg, J.; Zhu, T.; Vulcan, T.; Solonenko, M.; Rodriguez, C.; Chang, J.; Saunders, M.; Mason, N.; Hahn, S. *Clin. Cancer Res.* **2001**, *7*, 651–660.

(25) O'Connor, A. E.; William, M.; Gallagher, W. M.; Byrne, A. T. *Photochem. Photobiol.* **2009**, *85*, 1053–1074.

(26) Wainwright, M. *Chem. Soc. Rev.* **1996**, *25*, 351–359.

(27) New, O. M.; Dolphin, D. *Eur. J. Org. Chem.* **2009**, *16*, 2675–2686.

(28) Gorman, A.; Killoran, J.; O'Shea, C.; Kenna, T.; Gallagher, W. M.; O'Shea, D. F. *J. Am. Chem. Soc.* **2004**, *126*, 10619–10631.

(29) Roelants, M.; Lackner, B.; Waser, M.; Falk, H.; Agostinis, P.; Van Poppeland, H.; De Witte, P. A. M. *Photochem. Photobiol. Sci.* **2009**, *8*, 822–829.

(30) Will, S.; Rahbar, A.; Schmickler, H.; Lex, J.; Vogel, E. *Angew. Chem., Int. Ed. Engl.* **1990**, *29*, 1390–1393.

(31) Aritome, I.; Shimakoshi, H.; Hisaeda, Y. *Acta Crystallogr., Sect. C* **2002**, *58*, 563–564.

(32) Baba, T.; Shimakoshi, H.; Aritome, I.; Hisaeda, Y. *Chem. Lett.* **2004**, *33*, 906–907.

(33) Shimakoshi, H.; Baba, T.; Iseki, Y.; Aritome, I.; Endo, A.; Adachib, C.; Hisaeda, Y. *Chem. Commun.* **2008**, 2882–2884.

(34) Braslavsky, S. E.; Müller, M.; Mártire, D. O.; Pörting, S.; Bertolotti, S. G.; Chakravorti, S.; Koç-Weier, G.; Knipp, B.; Schaffner, K. *J. Photochem. Photobiol. B: Biol.* **1997**, *40*, 191–198.

(35) Casida, M. E. In *Recent Developments and Applications in Density-Functional Theory*; Seminario, J. M., Ed.; Elsevier: Amsterdam, 1996; pp 155−192.

(36) Werschnik, J.; Gross, E. K. U.; Burke, K. *J. Chem. Phys.* **2005**, *123*, 62206–62206(9).

(37) Elliott, P.; Burke, K.; Furche, F. In *Recent Advances in Density Functional Methods*; Lipkowitz, K. B., Cundari, T. R., Eds.; Wiley: Hoboken, NJ, 2009; Vol. 26, pp 91−165.

(38) Jacquemin, D.; Wathelet, V.; Perpète, E. A.; Carlo Adamo, C. *J. Chem. Theory Comput.* **2009**, *5*, 2420–2435, No. 9.

(39) Chiodo, S.; Russo, N. *J. Comput. Chem.* **2008**, *29*, 912.

(40) Chiodo, S. G.; Russo, N. *J. Comput. Chem.* **2009**, *30*, 832.

(41) Bethe, H. A.; Salpeter, E. E. *Quantum Mechanics of the One and Two Electron Atoms*; Plenum: New York, 1977.

(42) Chernyak, V.; Mukamel, S. *J. Chem. Phys.* **2000**, *112*, 3572.

(43) Send, R.; Furche, F. *J. Chem. Phys.* **2010**, *132*, 044107.

(44) Furche, F. *J. Chem. Phys.* **2001**, *114*, 5982.

(45) Tavernelli, I.; Tapavicza, E.; Rothlisberger, U. *J. Chem. Phys.* **2009**, *130*, 124107.

(46) Ahlrichs, R.; Bär, M.; Häser, M.; Horn, M.; Kölmel, C. *Chem. Phys. Lett.* **1989**, *162*, 165–169.

(47) Perdew, J. P.; Burke, K.; Ernzerhof, M. *Phys. Rev. Lett.* **1996**, *77*, 3865–3868.

(48) Perdew, J. P.; Ernzerhof, M.; Burke, K. *J. Chem. Phys.* **1996**, *105*, 9982–9985.

(49) Schwerdtfeger, P.; Dolg, M.; Schwarz, W. H. E.; Bowmaker, G. A.; Boyd, P. D. W. *J. Chem. Phys.* **1989**, *91*, 1762–1774.

(50) Schäfer, A.; Horn, H.; Ahlrichs, R. *J. Chem. Phys.* **1992**, *97*, 2571–2577.

(51) Deglmann, P.; Furche, F. *J. Chem. Phys.* **2002**, *117*, 9535-four pages.

(52) Grimme, S. *J. Chem. Phys.* **2006**, *124*, 34108.

(53) Schwabe, T.; Grimme, S. *Phys. Chem. Chem. Phys.* **2007**, *9*, 3397–3406.

(54) Weigend, F.; Häser, M.; Patzelt, H.; Ahlrichs, R. *Chem. Phys. Lett.* **1998**, *294*, 143.

(55) Bauernschmitt, R.; Ahlrichs, R. *Chem. Phys. Lett.* **1996**, *256*, 454–464.

(56) Gorelsky, S. I. SWizard program, revision 4.6, http://www.sg-chem.net/.

(57) Klamt, A.; Schüürmann, G. *J. Chem. Soc. Perkin Trans.2* **1993**, *5*, 799–805.

(58) Boese, A. D.; Martin, J. M. L. *J. Chem. Phys.* **2004**, *121*, 3405–16.

(59) Zhao, Y.; Truhlar, D. G. *Theor. Chem. Acc.* **2008**, *120*, 215–241.

(60) Frisch, M. J.; Trucks, G. W.; Schlegel, H. B.; Scuseria, G. E.; Robb, M. A.; Cheeseman, J. R.; Montgomery, J. A., Jr.; Vreven, T.; Kudin, K. N.; Burant, J. C.; Millam, J. M.; Scalmani, G.; Rega, N.; Petersson, G. A.; Nakatsuji, H.; Hada, M.; Ehara, M.; Toyota, K.; Fukuda, R.; Hasegawa, J.; Ishida, M.; Nakajima, T.; Honda, Y.; Kitao, O.; Nakai, H.; Klene, M.; Li, X.; Knox, J. E.; Hratchian, H. P.; Cross, J. B.; Bakken, V.; Adamo, C.; Jaramillo, J.; Gomperts, R.; Stratmann, R. E.; Yazyev, O.; Austin, A. J.; Cammi, R.; Pomelli, C.; Ochtersky, J. W.; Ayala, P. Y.; Morokuma, K.; Voth, G. A.; Salvador, P.; Dannenberg, J. J.; Zakrzewski, V. G.; Dapprich, S.; Daniels, A. D.; Strain, M. C.; Farkas, O.; Malick, D. K.; Rabuck, A. D.; Raghavachari, K.; Foresman, J. B.; Ortiz, J. V.; Cui, Q.; Baboul, A. G.; Clifford, S.; Cioslowski, J.; Stefanov, B. B.; Liu, G.; Liashenko, A.; Piskorz, P.; Komaromi, I.; Martin, R. L.; Fox, D. J.; Keith, T.; Al-Laham, M. A.; Peng, C. Y.; Nanayakkara, A.; Challacombe, M.; Gill, P. M. W.; Johnson, B.; Chen, W.; Wong, M. W.; Gonzalez, C.; Pople, J. A. *Gaussian 03*, revision B.05; Gaussian, Inc.: Wallingford, CT, 2004.

(61) Waluk, J. *Acc. Chem. Res.* **2006**, *39*, 945–952.

(62) Braun, J.; Schlabach, M.; Wehrle, B.; Köcher, M.; Vogel, E.; Limbach, H. H. *J. Am. Chem. Soc.* **1996**, *118*, 7231–7232.

(63) Gil, M.; Waluk, J. *J. Am. Chem. Soc.* **2007**, *129*, 1335–1341.

(64) Gil, M.; Jasny, J.; Vogel, E.; Waluk, J. *Chem. Phys. Lett.* **2000**, *323*, 534–541.

(65) Gouterman, M. *J. Mol. Spectrosc.* **1961**, *6*, 138–163.

(66) Gouterman, M.; Wagnière, G.; Snyder, L. *J. Mol. Spectrosc.* **1963**, *11*, 108–127.

(67) Platt, J. R. In *Radiation Biology*; Hollaender, A., Ed.; McGraw-Hill: New York, 1956; Vol. 3, pp 71−123.

(68) Toyota, K.; Hasegawa, J.; Nakatsuji, H. *Chem. Phys. Lett.* **1996**, *250*, 437–442.

(69) Edwards, L.; Dolphyn, D. H.; Gouterman, M.; Adler, A. D. *THEOCHEM* **1997**, *401*, 301–314.

(70) Hasegawa, J.; Takata, K.; Miyahara, T.; Neya, S.; Frisch, M.; Nakatsuji, H. *J. Chem. Phys. A* **2005**, *109*, 3187–3200.

(71) Waluk, J.; Müller, M.; Swiderek, P.; Köcher, M.; Vogel, E.; Hohlneicher, G.; Michl, J. *J. Am. Chem. Soc.* **1991**, *113*, 5511–5527.

CT100287G